Advanced Steel Construction – Vol. 18 No. 4 (2022) 736–744
DOI:10.18057/IJASC.2022.18.4.1

A MODEL FOR PREDICTING MOMENT-CURVATURE BEHAVIOR OF SELF-STRESSING SSACFST COLUMNS UNDER LOW CYCLIC LOADING

Feng Yu [1], Yue Cao [1], Yuan Fang [1, 2, *], Yuan-Di Qian [1, 3], Chi Yao [1] and Yin Qin [1]

[1] *Department of Civil Engineering and Architecture, Anhui University of Technology, Ma'anshan, China*
[2] *Key Laboratory of Metallurgical Emission Reduction & Resources Recycling (Anhui University of Technology), Ministry of Education*
[3] *China MCC 17 Group Co., Ltd*
**(Corresponding author: Email: fyuan86@126.com)*

ABSTRACT

This paper reports the experimental investigation and theoretical model of self-stressing steel slag aggregate concrete-filled steel tubular (SSACFST) columns under low cyclic loading. Fourteen specimens including ten self-stressing SSACFST columns and four ordinary SSACFST columns (reference columns) are tested, and the effects of four experimental variables, such as axial compression ratio (n), diameter-thickness ratio (D/t_s), shear-span ratio (λ), and expansion rate (P_{ct}) of steel slag aggregate concrete (SSAC) on failure mode, moment-curvature hysteretic curves and skeleton curves are examined. Experimental results demonstrate that the failure mode of columns with high shear-span ratio is bending failure while the bending-shear failure dominates the damage of columns with low shear-span ratio. With the enhancement of axial compression ratio or expansion rate of SSAC, the peak moment of specimens increases. The increase of shear-span ratio or diameter-thickness ratio decreases the peak moment of specimens. The peak curvature of specimens decreases as axial compression ratio increases, while it increases as shear-span ratio increases. The impacts of diameter-thickness ratio and expansion rate of SSAC on peak curvature of specimens are marginal. A simplified calculation method of moment-curvature skeleton curves is suggested and the hysteresis rules of self-stressing SSACFST columns are also proposed by analyzing the features of hysteretic curves. Ultimately, a model for evaluating moment-curvature behavior of self-stressing SSACFST columns under low cyclic loading is established and validated the experimental results with good agreement.

ARTICLE HISTORY

Received: 22 June 2021
Revised: 18 March 2022
Accepted: 27 March 2022

KEYWORDS

Concrete filled steel tube;
Steel slag aggregate concrete;
Self-stressing;
Low cyclic loading;
Moment-curvature

1. Introduction

Steel slag is main industrial waste produced in steel-making process. In developing countries, especially in China, the emissions of steel slag reaches more than 100 million tons per year, while the utilization rate of steel slag is only 29.5% [1]. Numerous accumulated steel slag not only occupies land resources, but also gives rise to environmental pollution. Therefore, the reasonable and scientific treatment of these steel slag wastes has attracted the attention of researchers.

Currently, an increasing number of scholars use steel slag as fine aggregate[2], coarse aggregate [3-4] or both fine and coarse aggregates [5] to prepare SSAC, and a large number of investigations have been conducted [6-8]. These investigations prove that the steel slag can meet the requirements of concrete aggregate and SSAC will be a potential treatment method of steel slag wastes, which will bring satisfactory environmental and economic effects. The benefits of using SSAC are listed in Table 1.

Table 1
The benefits of using SSAC

	SSAC
Benefits	Reduce land occupation, alleviate environmental pollution, significant environmental benefits
	Recycle solid waste, reduce natural aggregate consumption, considerable economic benefits
	Excellent mechanical properties
	Favorable durability
	Low hydration heat

Qasrawi et al. [9] used steel slag as fine aggregate in the concrete mix and found that the 28-day compressive and and tensile strength was improved by 1.1~1.3 and 1.4~2.4 times, respectively, depending on concrete grade and sand replacement ratio. Maslehuddin et al. [10] conducted the experimental study on durability of SSAC and demonstrated that the durability of SSAC was superior than that of crushed limestone aggregate concrete. However, SSAC is not widely used in structural engineering. This results arises because SSAC potentially contains high contents of free CaO and MgO, which expand when hydrated, the generated internal pressure causes surface cracks and protrusion [11]. To this end, scholars have proposed some stabilization measures to inhibit the volume expansion of SSAC, such as carbonation of steel slag [12], phosphoric acid modification [13] and reduction of MgO and free CaO contents [14].

Concrete-filled steel tubular (CFST) column has been extensively applied in bridge engineering, power transmission towers, and high-rise buildings due to its significant merits of high load capacity, favorable ductility and convenient construction. Numerous experimental and theoretical investigations on CFST columns have been performed and fruitful research results have been achieved [15-17]. However, the hardening shrinkage of core concrete may reduce the durability and affect the safety of structure. To solve this problem, a self-stressing CFST column formed by pouring expansive concrete into steel tube has been proposed and a lot of experimental studies have been conducted [18-19]. Li et al. [20] tested the self-stressing CFST columns under axial compression and demonstrated that the ultimate bearing capacity increased by 9.8%-27.6% compared with ordinary CFST columns. Chang et al. [21] studied the mechanical performances of self-stressing CFST columns under eccentric load and revealed that the bearing capacity of self-stressing CFST columns was generally higher than that of ordinary CFST columns and it decreased with the increase of eccentricity.

As mentioned above, the existence of the self-stressing alleviates the impact of shrinkage on the mechanical behavior of CFST column and improves its co-operative working ability. At present, the expansive concrete prepared by adding additives can compensate volume shrinkage and form self-stressing in steel tubes. However, the incorporation of additives increases the construction cost and complicates the hydration and hardening process of concrete.

In recent years, scholars have poured expanded SSAC into steel tubes to prepare self-stressing SSACFST members and conducted the relevant theoretical and experimental investigations [22-23]. Considering the impact of the diameter-thickness ratio, expansion rate of SSAC and eccentricity, Yu et al. [24] experimentally investigated the static performances of self-stressing SSACFST columns, revealed the failure mode of the axially or eccentrically loaded self-stressing SSACFST columns, and proposed the corresponding prediction formulas of ultimate bearing capacity. Fang et al. [25] reported the axial compressive behavior of self-stressing SSACFST short and medium long columns, and proposed the calculation formulas of bearing capacity. Yu et al. [26] investigated the axial compressive behavior of self-stressing SSACFST columns with different loading modes and evaluated the rationality of existing CFST design formulas to estimate their bearing capacity. These investigations confirmed that the self-stressing SSACFST columns not only alleviates the shrinkage of core concrete in steel tubes, but also effectively recycles steel slag wastes. In addition, to capitalize on the volume expansion of SSAC, a SSAC filled-FRP tube column was proposed in recent research [27] and its physical and mechanical properties were systematically tested.

Obviously, a series of studies on the static performances of self-stressing SSACFST columns have been conducted and considerable results have been obtained. However, research on seismic performance of self-stressing

SSACFST columns is rarely reported. To further reveal the seismic response of this novel composite column, fourteen specimens including ten self-stressing SSACFST columns and four ordinary SSACFST columns (reference columns) are tested. The effects of the axial compression ratio (n), diameter-thickness ratio (D/t_s), shear-span ratio (λ), and expansion rate (P_{ct}) on failure modes, moment-curvature hysteretic curves and skeleton curves are examined. Additionally, an analytical model for predicting moment-curvature behavior of self-stressing SSACFST columns under low cyclic loading is established and validated the experimental results with good agreement.

2. Experimental program

2.1. Specimen design

In this study, ten self-stressing SSACFST columns and four ordinary SSACFST columns (reference columns) are designed and fabricated. To reveal the impacts of P_{ct} on seismic response of self-stressing SSACFST columns under low cyclic loading, an expansive SSAC with P_{ct}=11.1×10^{-4} and a reference SSAC with P_{ct}=-3.4×10^{-4} are designed and used in the experiments. The detailed composition of two types of SSAC are listed in Table 2. The particle size range of steel slag sand and coarse steel sand are 0~4.75mm, and 4.75~26.5 mm, respectively. The photos of steel slag aggregates are shown in Fig .1.

Three other tested variables are also considered, such as axial compression ratio (i.e., n = 0.2 and 0.4), diameter-thickness ratio (i.e., D/t_s= 44.88, 58.71 and 76.84), and shear-span ratio (i.e., λ = 0.91, 1.37 and 1.83). The expansion rate of SSAC is measured in accordance with the method suggested in Chinese code GB/T50082-2009 [28], 100 mm×100 mm×300 mm prismatic specimens are selected. The first group length is measured after 3 days of curing and counted as the initial length of specimens L_0, and thereafter the lengths of the specimens are measured daily and counted as length L_t. The free expansion rate of SSAC can be calculated by Eq (1).

$$P_{ct}=(L_t-L_0)/L_b \quad (1)$$

where, P_{ct} is the free expansion rate of SSAC on day t, L_b is the standard distance of the specimens.

The mineral composition of steel slag are measured by X-ray diffraction and X-ray fluorescence spectrometry, as listed in Table 3. All the specimens are designed to be I-shaped with a total height of 1600 mm. The appearance, dimension and configuration of reinforcement are shown in Fig. 2. Specimen manufacturing process is depicted in Fig. 3. The detailed design parameters of specimens are listed in Table 4.

Table 2
Detailed mechanical properties of SSAC

Type of concrete	Water cement ratio	Material usage / kg.m^{-3}				
		Water	Cement	Steel slag sand	Gravel	Coarse steel slag
Self-stressing SSAC	0.5	189.8	396.3	779.6	777.8	261.1
Reference SSAC	0.58	189.8	326.9	780.6	0	1038.9

Table 3
Mineral composition of steel slag

Mineral composition	CaO (%)	SiO_2 (%)	Al_2O_3 (%)	Fe_2O_3 (%)	MgO (%)	SO_3 (%)	TiO_2 (%)	MnO (%)
Steel slag	52.71	12.97	2.12	19.53	4.31	0.3	1.59	2.21

(a) Steel slag sand

(b) Coarse steel slag

Fig. 1 Photos of steel slag aggregates

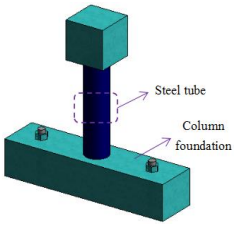

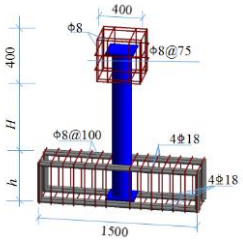

Fig. 2 The dimension of the columns and reinforcement skeleton (unit: mm)

(a) Binding of steel skeleton

(b) Template installation

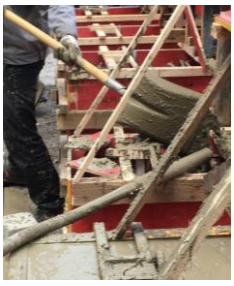

(c) Pouring of concrete

(d) Curing of specimen

Fig. 3 Specimen manufacturing process

Table 4
Experimental parameters of the specimens

Specimen	H /mm	D /mm	t_s /mm	n	D/t_s	λ	P_{ct} /10^{-4}
S1-1	800	219	2.85	0.2	76.84	1.83	11.1
S1-2	800	219	3.73	0.2	58.71	1.83	11.1
S1-3	800	219	4.88	0.2	44.88	1.83	11.1
S1-4	600	219	2.85	0.2	76.84	1.37	11.1
S1-5	400	219	2.85	0.2	76.84	0.91	11.1
S1-6	800	219	2.85	0.4	76.84	1.83	11.1
S1-7	800	219	3.73	0.4	58.71	1.83	11.1
S1-8	800	219	4.88	0.4	44.88	1.83	11.1
S1-9	600	219	2.85	0.4	76.84	1.37	11.1
S1-10	400	219	2.85	0.4	76.84	0.91	11.1
S2-1	800	219	2.85	0.2	76.84	1.83	-3.4
S2-2	600	219	2.85	0.2	76.84	1.37	-3.4
S2-3	400	219	2.85	0.2	76.84	0.91	-3.4
S2-4	800	219	2.85	0.4	76.84	1.83	-3.4

Note: H is column length, D denotes outer diameter of steel tube, t_s represents thickness of steel tube.

2.2. Mechanical properties of the materials

The mechanical properties of steel tube and SSAC are measured based on the suggested test methods in Chinese code GB/T228.1-2010 [29] and GB/T 50081-2019 [30], respectively. The measured average yield tensile strength of steel tubes with thickness of 2.85 mm, 3.73 mm and 4.88 mm are 336 MPa, 314 MPa, 308 MPa, and the corresponding ultimate tensile strength are 561 MPa, 532 MPa and 504 MPa, respectively. Fig. 4 depicts the measured stress-strain curves of steel tubes with three different thickness. In this figure, σ_s is the compressive stress of steel tube, ε_z and ε_h represent the circumferential and axial strains, respectively. The compressive strength of the reference SSAC and self-stressing SSAC are 38.27 MPa, 38.40 MPa, and the corresponding elastic modulus are 2.953×10^4 MPa and 2.958×10^4 MPa, respectively.

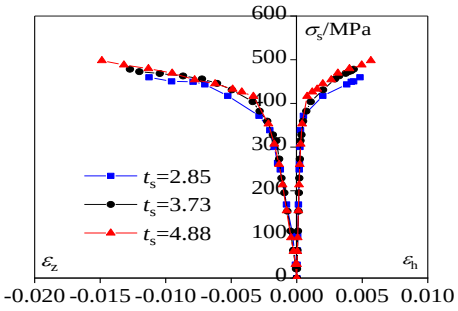

Fig. 4 Stress-strain curves of steel tubes

2.3. Test setup and loading scheme

The constant axial load and the horizontal cyclic load are respectively applied by a 2000 kN hydraulic jack and a 500 kN MTS electro-hydraulic servo actuator on the top of specimens. Initially, single-stage cyclic displacement loading scheme is adopted and the displacement increment is 1 mm. After yielding, single-stage cyclic displacement loading scheme is switched to three-stage cyclic displacement loading, and the displacement of each stage is an integral multiple of the yield displacement. When the horizontal bearing capacity drops to 85% of the ultimate strength, the test is terminated.

3. Experimental results analysis

3.1. Failure modes

According to the test results, the failure modes of columns with low shear-span ratios (i.e., λ=0.91and 1.37) were basically similar, which were manifested as bending-shear failure, whereas the bending failure dominated the damage of columns with high shear-span ratio (i.e., λ=1.83). The impacts of other three experimental variables (n, D/t_s, and P_{ct}) on the final failure mode were marginal.

In the present study, specimen S1-4 was taken as an example to specify the failure characteristics of the low shear-span ratio specimens. As shown in Fig. 5, the steel tube yielded within 150 mm from the bottom of column. The local buckling appeared about 21 mm away from the bottom of column, where the steel tube formed a two-way drum wave and a horizontal crack was developed at the crest of wave. After experiment, the outer steel tube was stripped, and it was found that the core SSAC was crushed within 40 mm from the bottom of column and presented obvious granular slag. The fracture degree of core SSAC decreased as the n or P_{ct} increased. Besides, a few circumferential and oblique cracks appeared at the bottom of the column, and the width and depth of the cracks were small. No obvious cracks appeared in other parts of the column.

Compared with low shear-span ratio specimens, the steel tube yield range of columns with high shear-span ratio was larger, the local buckling of steel tube was more distinct and the concrete crushing range was larger. Taking the specimen S1-1 as an example, the steel tube yielded within 200 mm from the bottom of column. The yield range of steel tube in specimen S1-1 was approximately 1.33 times than that of in specimen S1-4. The local buckling appeared about 120 mm away from the bottom of column, where the steel tube formed a two-way drum wave and a horizontal crack was developed at the crest of wave. With the increase of the n or P_{ct}, the buckling degree of steel tube decreased, while the influence of the D/t_s on it was insignificant. Similarly, the outer steel tube was peeled off and it was found that the core SSAC was crushed within 50 mm from the bottom of column and presented distinct powder slag. In contrast, the concrete crushing degree of the high shear-span ratio columns was less serious than that of the low shear-span ratio specimens. A small number of circumferential cracks appeared at the bottom of columns, while no distinct cracks appeared in other parts of the columns. The integrity of the core SSAC columns was favorable. The typical failure mode of column with high shear-span ratio is shown in Fig. 6.

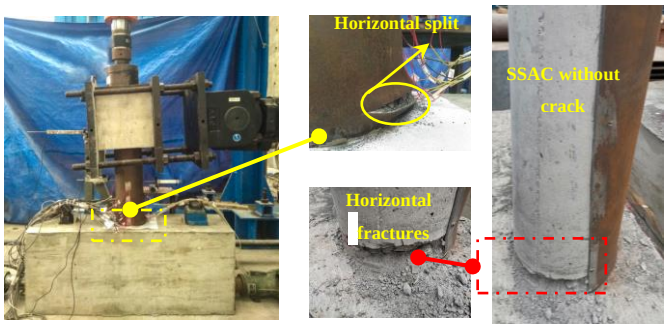

(a) Overall failure mode (b) Local failure mode

Fig. 5 The typical failure mode of column with low shear-span ratio (S1-4)

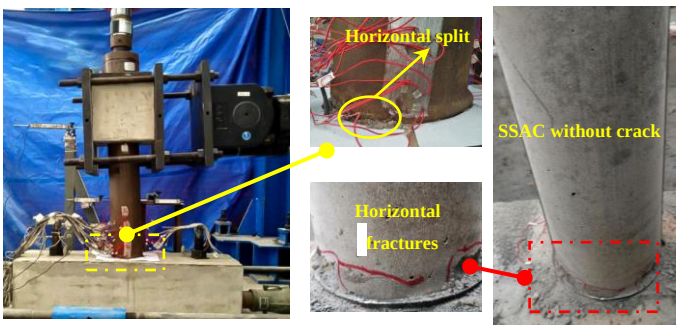

(a) Overall failure mode (b) Local failure mode

Fig. 6 The typical failure mode of column with high shear-span ratio (S1-1)

3.2. Moment-curvature hysteretic curves

The moment-curvature hysteretic curves $M-\phi$ of the specimens are shown in Fig. 7. Initially, all specimens show elastic response, moment and curvature increase linearly, and stiffness degradation is not apparent. Meanwhile, the hysteretic loop area is relatively small. As the load increases, the $M-\phi$ hysteretic curves gradually deviate from the linearity, and the columns come into elastic-plastic stage. At this stage, the hysteretic curves exhibit remarkable fusiform shape, and the hysteretic loop area significantly increases. In plastic stage, the $M-\phi$ hysteretic curves present slight pinch phenomenon when the columns reach the ultimate bearing capacity. The hysteretic loop shape is still similar to fusiform, indicating that the columns show satisfactory energy dissipation capacity.

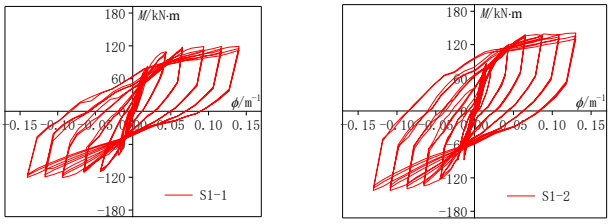

(a) S1-1 (b) S1-2

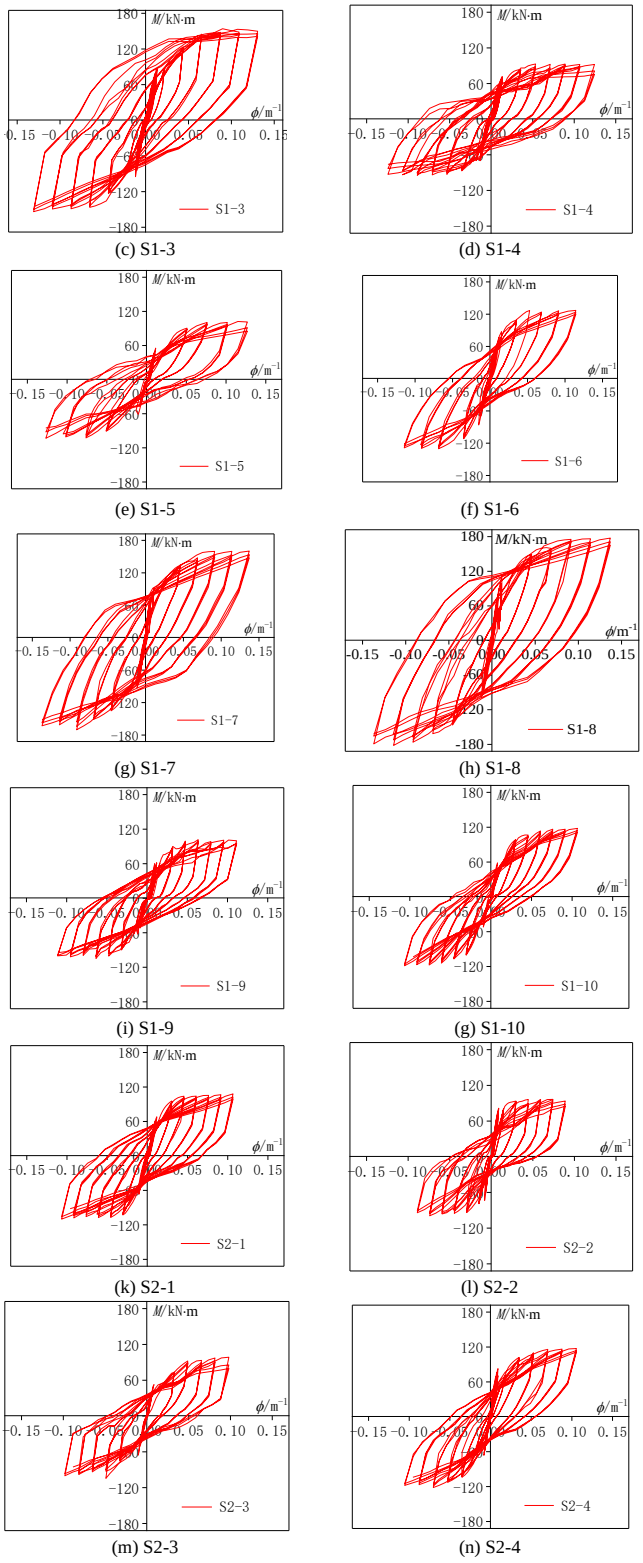

(c) S1-3 (d) S1-4

(e) S1-5 (f) S1-6

(g) S1-7 (h) S1-8

(i) S1-9 (g) S1-10

(k) S2-1 (l) S2-2

(m) S2-3 (n) S2-4

Fig. 7 The $M-\phi$ hysteresis curves

3.3. Moment-curvature skeleton curves analysis

The $M-\phi$ skeleton curves of self-stressing SSACFST columns are approximately divide into rising and stable stages. In the rising stage, the $M-\phi$ skeleton curves of the specimens increase linearly. As the moment reaches 61%~73% of the ultimate moment, the $M-\phi$ skeleton curves deviate from the linear growth and the turning points appear. As load further increases, the slope of $M-\phi$ skeleton curves decreases gradually and eventually the moment nearly remains constant.

3.3.1. Effect of axial compression ratio

As can be seen from Fig. 8(a), with the enhancement of *n*, the initial stiffness of columns increases, the peak moment increases while the peak curvature decreases. For example, the peak moment of specimen S1-6 increases by 12.7% compared with that of specimen S1-1. This is because increasing the *n*, the lateral stiffness of the column increases, and the ability to resist deformation is strengthened. After reaching the peak moment, the slope of $M-\phi$ skeleton curves of columns with an axial compression ratio of 0.2 decreases relatively slowly compared with those with an axial compression ratio of 0.4, indicating that columns with lower axial compression ratio have better ductility. With the increase of the *n*, the stiffness degradation accelerates and the ductility decreases.

3.3.2. Effect of the shear-span ratio

Fig. 8(b**)** depicts the effect of the λ on $M-\phi$ skeleton curves of the columns. The initial $M-\phi$ skeleton curves are approximately coincident, indicating that the λ has little impact on the initial stiffness. As the λ decreases, the peak moment of columns increases. Compared with specimen S1-1, the peak moment of specimen S1-5 increases by 30.1%. After reaching the peak moment, for the columns with low λ, the descending section of skeleton curves is steeper. The columns with high λ shows favorable ductility and their peak moment decreases slowly. With the decrease of the λ, the effective height of columns decreases, the horizontal shear stress of the column section increases, and the ultimate curvature decreases.

3.3.3. Effect of the diameter-thickness ratio

As illustrated in Fig. 8(c), the initial stiffness of columns with different D/t_s is basically the same. With the decrease of the D/t_s, the peak moment of columns increases, whereas, the impact of D/t_s on the peak curvature is marginal. When the D/t_s decreases from 76.84 (S1-1) to 44.88 (S1-3), the peak moment and peak curvature increase by 58.1% and 5.1%, respectively. The reason is that decreasing the D/t_s increases the steel ratio of specimen, the confinement effect of the outer steel tube on core SSAC is strengthened, the moment resistance of the columns is enhanced.

3.3.4. Effect of the expansion rate of SSAC

As shown in Fig. 8(d), at the initial of loading, specimen with larger P_{ct} shows higher stiffness. This result proves that the existence of self-stressing is beneficial to improve the lateral stiffness of the columns. With the increase of the P_{ct}, the peak moment increases. In contrast, the impact of the P_{ct} on the peak curvature is marginal. For instance, the peak moment and peak curvature of specimen S1-2 increases by 13.6% and 2.4% compared with those of specimen S2-2. This may be due to the fact that with the increase of the P_{ct}, the core SSAC is always in a tri-axial stress state, and the self-stressing makes the outer steel tube have a stronger confinement on core SSAC.

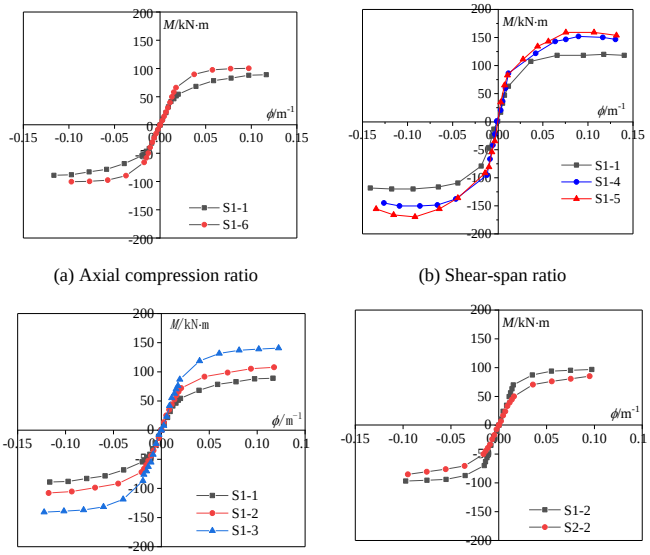

(a) Axial compression ratio (b) Shear-span ratio

(c) Diameter-thickness ratio (d) Expansion rate of SSAC

Fig. 8 Effect of variable parameters on $M-\phi$ skeleton curves

4. Analytical modeling of moment-curvature

4.1. A model for predicting the $M-\phi$ skeleton curves

In this section, a model for conveniently predicting the $M-\phi$ skeleton curves is proposed based on tri-linear skeleton model of CFST members. The calculated yield peak and ultimate points are connected to form a simplified $M-\phi$ skeleton curve, as shown in Fig. 9.

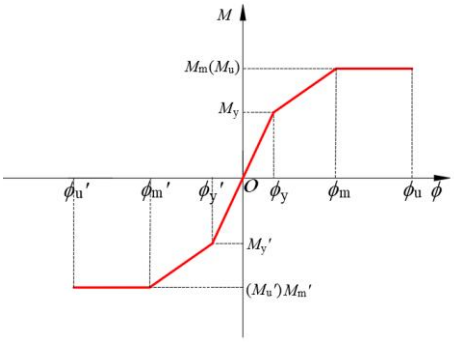

Fig. 9 Simplified $M-\phi$ skeleton curve

4.1.1. Basic assumptions

To develop the simplified $M-\phi$ skeleton curve model, the following assumptions are made.

(1) The self-stressing SSACFST column section conforms to the plane-section hypothesis.

(2) The tensile action of core SSAC is neglected.

(3) The relative slip between steel tube and SSAC is ignored.

(4) The constitutive relationship models of steel tube and self-stressing SSAC are respectively adopted in references [31-32].

4.1.2. Parameters determination

To accurately establish the above simplified $M-\phi$ skeleton model, several key characteristic points, such as yield moment (M_y), yield curvature (ϕ_y), peak moment (M_m), peak curvature (ϕ_m), ultimate moment (M_u) and ultimate curvature (ϕ_u), are needed to be determined.

(1) Yield moment (M_y)

According to the measured strain values, the circumferential stress of steel tube can be calculated, as shown below.

$$\sigma_h=\frac{E_s}{1+\nu^2}(\varepsilon_h+\nu\varepsilon_z) \tag{2}$$

where, σ_h is circumferential stress of steel tube, ε_h and ε_z are measured circumferential strain and longitudinal strain of steel tube, respectively, ν is Poisson's ratio.

The initial self-stressing of core SSAC can be determined as follows.

$$\sigma_0=\frac{t_s}{R_c}\sigma_h \tag{3}$$

In which, σ_0 is self-stressing of core SSAC and R_c is inner radius of core SSAC.

The yield moment of self-stressing SSACFST columns can be determined by the following formula.

$$M_y=\frac{f_{co}A_c}{\pi}\left(\frac{2}{3}\mu R_c\cos^3\theta_y+(R_c+R_s)\,\xi\cos\theta_y\right) \tag{4}$$

where θ_y denotes correlation angle of compression zone corresponding to the yield of specimens, $\theta_y=\frac{2.674\mu-2n\pi(\xi+1)}{4\xi+1.849\mu}$, R_s is cross-sectional radius of circular steel tube, ξ is constraint effect coefficient, $\xi=f_yA_s/f_{co}A_c$, $f_{co}=0.67f_{cu}$, $\mu=1+4\frac{\sigma_0}{f_{co}}$, μ represents self-stressing enhancement coefficient.

(2) Yield curvature (ϕ_y)

In this study, the stiffness of specimens is determined according to EC4 (2004) [33], and the calculation formula can be expressed as follows.

$$K_e=E_sI_s+0.6E_cI_c \tag{5}$$

In which, I_c represents the inertia moment of core SSAC section, $I_c=\frac{\pi(D-t_s)^4}{64}$, I_s denotes the cross-section inertia moment of outer steel tube, $I_s=\frac{\pi D^4}{64}-I_c$.

The calculation formula of yield curvature can be determined as:

$$\phi_y=\frac{M_y}{K_e} \tag{6}$$

(3) Peak moment (M_m)

The constraint force of axial compression specimens can be determined by the following formula [34] .

$$P_0=\frac{0.067\alpha f_y}{1.2+0.2\alpha} \tag{7}$$

where α is steel ratio, $\alpha=A_s/A_c$.

The non-uniformity coefficient γ is introduced and the relationship between the equivalent constraint force P_e and constraint force is established, as shown below.

$$P_e=\gamma P_0 \tag{8}$$

$$\gamma=-942.1\eta^2+146.76\eta+3.62 \tag{9}$$

$$\eta=\sigma_0/f_{co} \tag{10}$$

In which, η is the self-stressing level of core SSAC.

The calculation formula of the peak moment of self-stressing SSACFST columns is as follows.

$$M_m=\frac{f_{co}A_c}{\pi}G(\theta,\xi,\mu,\psi) \tag{11}$$

$$G(\theta,\xi,\mu,\psi)=\frac{2}{3}\mu' R_c\cos^3\theta+\psi\xi(R_c+R_s)\cos\theta \tag{12}$$

$$\psi=0.737n+1.376\eta-0.00067D/t_s+1.166 \tag{13}$$

$$\mu'=\mu+4P_e/f_{co} \tag{14}$$

(4) Peak moment (ϕ_m)

The stiffness of the elastic-plastic section of moment-curvature curves is shown in the following formula.

$$K_s=2792-42.1D/t_s+2034\eta+4223n \tag{15}$$

where, K_s is linear elastic-plastic segment stiffness.

The peak curvature of self-stressing SSACFST columns is determined as follows.

$$\phi_m=\frac{M_m-M_y}{K_s}+\phi_y \tag{16}$$

(5) Ultimate moment (M_u)

In this analysis, to simplify the calculation, it is considered that the peak moment of the columns is equal to the ultimate moment, $M_u=M_m$.

(6) Ultimate curvature (ϕ_u)

According to the test results, the self-stressing SSACFST column section meets the assumption of plane-section during the loading process. The ultimate curvature can be calculated by the following formula.

$$\phi_u = \frac{\varepsilon_{cu}}{R_c(1-\sin\theta)} \tag{17}$$

where, ε_{cu} is the ultimate strain of core SSAC, ε_{cu}=$110\alpha+0.015\sqrt{f_{cp}}$, $f_{cp}=\mu f_{co}+4P_e$, $\theta=\frac{|2.674\mu'-2n\pi(\xi+1)|}{4\psi\xi+1.849\mu'}$.

4.1.3. Evaluation of the proposed model

The comparisons between the experimental $M-\phi$ skeleton curves and theoretical $M-\phi$ skeleton curves are shown in Fig. 10. Clearly, the theoretical $M-\phi$ skeleton curves are close to the experimental results, demonstrating that the above proposed model has an acceptable precision.

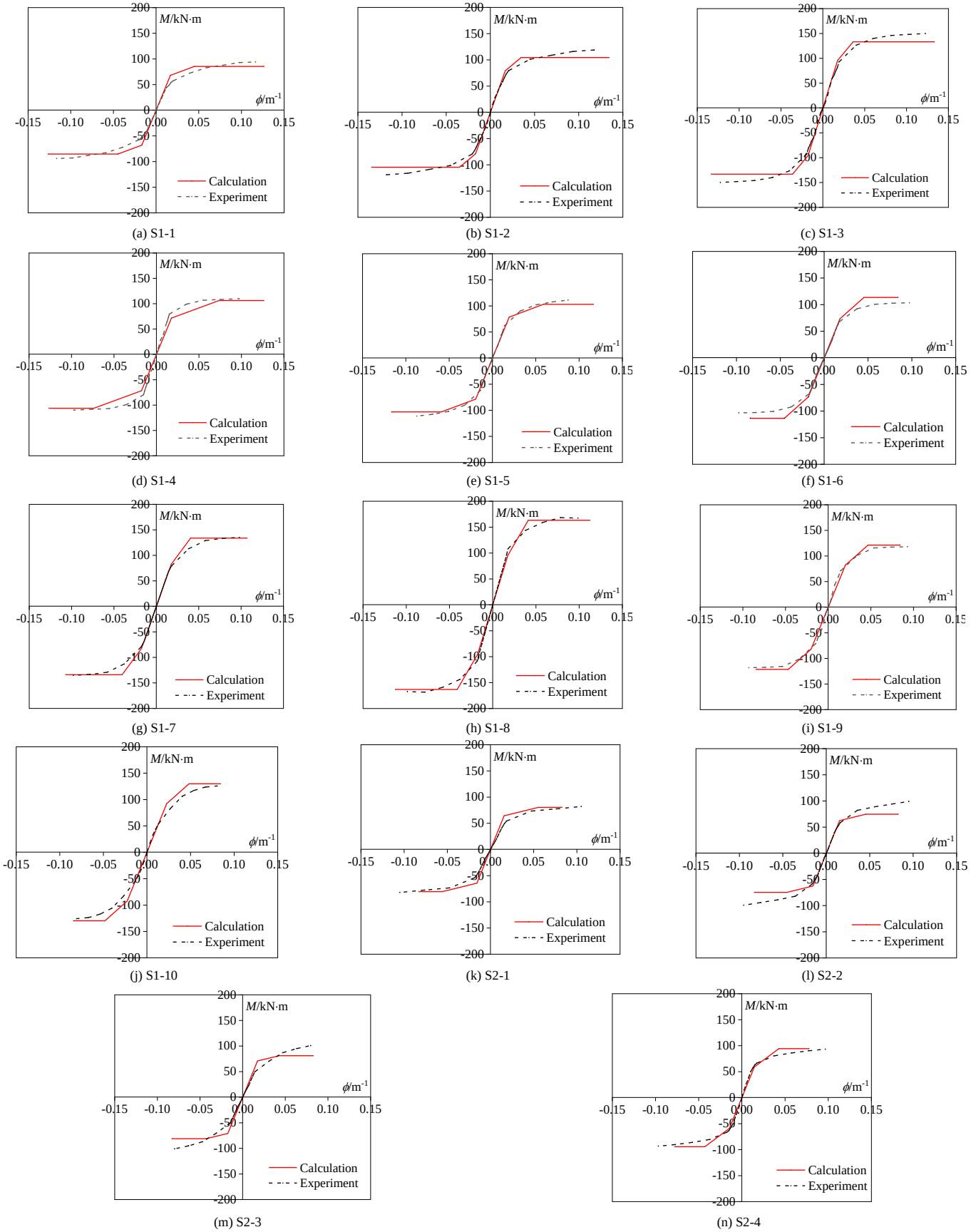

Fig. 10 The comparisons between the experimental $M-\phi$ skeleton curves and theoretical $M-\phi$ skeleton curves

4.2. Hysteresis rules

To establish a complete model for estimating moment-curvature behavior of self-stressing SSACFST columns, the hysteresis rules are required to be analyzed. As shown in Fig. 11, according to the degradation three-line model, five key parameters, such as elastic stiffness (K_e), moment at point A (M_1), yield moment (M_y), yield curvature (ϕ_y), and stiffness corresponding to the third stage (K_p), needed to be further determined. The specific calculation results are shown in Table 5.

(1) Elastic stiffness

To simplify the analysis, the elastic stiffness (K_e) is calculated according to EC4 (2004) [33] in this study, as shown in Eq (5).

(2) Moment at point A

The moment at point A can be determined by the following equation [32].

$$M_1 = 0.6M_y \tag{18}$$

(3) Yield moment and yield curvature

In this analysis, the yield moment M_y and the yield curvature ϕ_y can be calculated by Eq (4) and Eq (6).

(4) Stiffness corresponding to the third stage

Stiffness corresponding to the third stage K_p is the slope of connecting line segment between the yield point (M_y, ϕ_y) and ultimate point (M_u, ϕ_u) on skeleton curves, which can be calculated by the following formula.

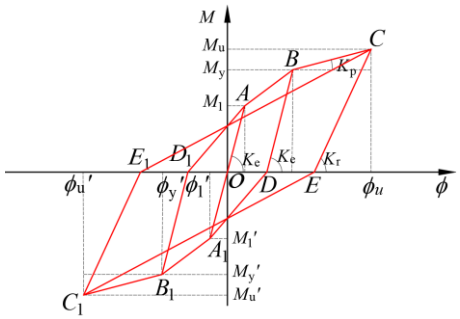

Fig. 11 Loading and unloading rules of the self-stressing SSACFST columns under low cyclic loading

$$K_p = \frac{M_u - M_y}{\phi_u - \phi_y} \tag{19}$$

(5) Softening stage

When the specimen is in elastic stage, the influences of stiffness degradation and residual deformation are ignored, the unloading curve is taken as an oblique line. At this stage, the unloading stiffness is equal to the elastic stiffness, $K_r = K_e$. When the specimen exceeds the elastic stage, the following unloading stiffness calculation formula K_r can be used to consider the degradation of component stiffness.

$$K_r = a_1 K_e \left(\frac{\phi_1}{\phi_y}\right)^{b_1} \tag{20}$$

where K_r is unloading stiffness, ϕ_1 is curvature corresponding to the unloading point of the *i*-th cyclic stiffness, a_1 and b_1 are the calculated parameters, which are related to n, λ and initial self-stressing σ_0.

$$a_1 = -2.34n + 0.93\lambda + 0.013D/t_s + 0.614\sigma_0 - 1.75 \tag{21}$$

$$b_1 = 0.27n - 0.11\lambda - 0.01D/t_s - 0.37\sigma_0 + 1.74 \tag{22}$$

4.3. Verification of the proposed model

On the basis of the skeleton curve prediction model and hysteresis rules, a model for predicting the $M-\phi$ hysteresis curves of self-stressing SSACFST columns is established. The comparisons between the experimental and theoretical $M-\phi$ hysteresis curves are shown in Fig. 12. It can be seen that the theoretical curves agree well with the experimental curves.

Table 5
Unloading stiffness of the specimens

ID		Variations of unloading stiffness of specimens											
S1-1	ϕ_i/ϕ_y	1.07	2.46	3.96	5.03	6.58	8.48	9.32	11.19				
	K_r/K_e	1.63	1.63	1.57	1.51	1.44	1.35	1.16	0.96				
S1-2	ϕ_i/ϕ_y	1.06	2.33	2.99	3.66	4.32	5.19	6.05	6.91	7.77	8.64	9.66	10.33
	K_r/K_e	1.77	1.78	1.78	1.69	1.61	1.61	1.56	1.57	1.57	1.46	1.37	1.18
S1-3	ϕ_i/ϕ_y	1.01	2.57	3.36	4.14	4.93	5.91	6.90	7.89	8.87	9.86	10.79	12.57
	K_r/K_e	1.96	2.01	1.99	1.94	1.88	1.83	1.81	1.84	1.77	1.76	1.76	1.68
S1-4	ϕ_i/ϕ_y	1.04	1.27	2.91	3.54	4.18	4.81	5.44	6.06	6.69	7.32		
	K_r/K_e	1.14	1.14	1.09	0.98	1.00	1.03	0.98	0.88	0.8	0.77		
S1-5	ϕ_i/ϕ_y	1.13	3.26	4.39	5.52	6.65	7.54	8.42	9.30	10.19	11.07		
	K_r/K_e	1.09	1.00	0.96	1.00	0.90	0.89	0.82	0.86	0.84	0.83		
S1-6	ϕ_i/ϕ_y	1.10	2.4	3.09	3.79	4.49	5.09	5.68	6.28	6.87	7.47	9.10	11.4
	K_r/K_e	1.61	1.64	1.55	1.51	1.47	1.51	1.45	1.38	1.33	1.31	1.31	1.34
S1-7	ϕ_i/ϕ_y	1.12	3.84	5.26	6.68	8.10	8.91	9.72	10.53	11.34	12.16	12.42	13.84
	K_r/K_e	1.63	1.65	1.58	1.52	1.56	1.41	1.42	1.43	1.24	1.21	1.23	1.15
S1-8	ϕ_i/ϕ_y	1.25	3.5	4.75	6.00	7.25	7.98	8.70	9.42	10.15	10.87	12.25	13.5
	K_r/K_e	1.86	1.54	1.35	1.17	1.10	1.11	1.17	1.19	1.20	1.42	1.22	1.24
S1-9	ϕ_i/ϕ_y	1.04	2.28	2.93	3.57	4.21	4.84	5.47	6.11	6.74	7.37		
	K_r/K_e	1.21	1.21	1.18	1.18	1.17	1.05	1.06	1.06	1.06	1.00		
S1-10	ϕ_i/ϕ_y	1.12	5.24	7.35	9.47	10.42	11.36	12.31	13.26	14.26			
	K_r/K_e	1.04	0.95	0.85	0.79	0.79	0.80	0.89	0.85	0.82			
S2-1	ϕ_i/ϕ_y	1.08	2.15	2.73	3.30	3.88	4.92	5.95	6.99	8.03	9.06		
	K_r/K_e	2.28	2.38	2.21	2.57	2.51	1.61	1.41	1.37	1.13	0.97		
S2-2	ϕ_i/ϕ_y	1.02	3.84	5.26	6.68	7.52	8.35	9.18	10.02				
	K_r/K_e	1.72	1.55	1.46	1.44	1.39	1.31	1.35	1.33				
S2-3	ϕ_i/ϕ_y	1.01	4.22	5.83	7.44	8.37	9.30	10.23	11.16				
	K_r/K_e	1.58	1.31	1.11	0.94	1.00	1.07	1.05	1.03				
S2-4	ϕ_i/ϕ_y	1.11	4.33	5.99	7.65	8.63	9.60	10.58	11.55				
	K_r/K_e	1.13	1.14	0.96	0.89	0.86	0.83	0.77	0.78				

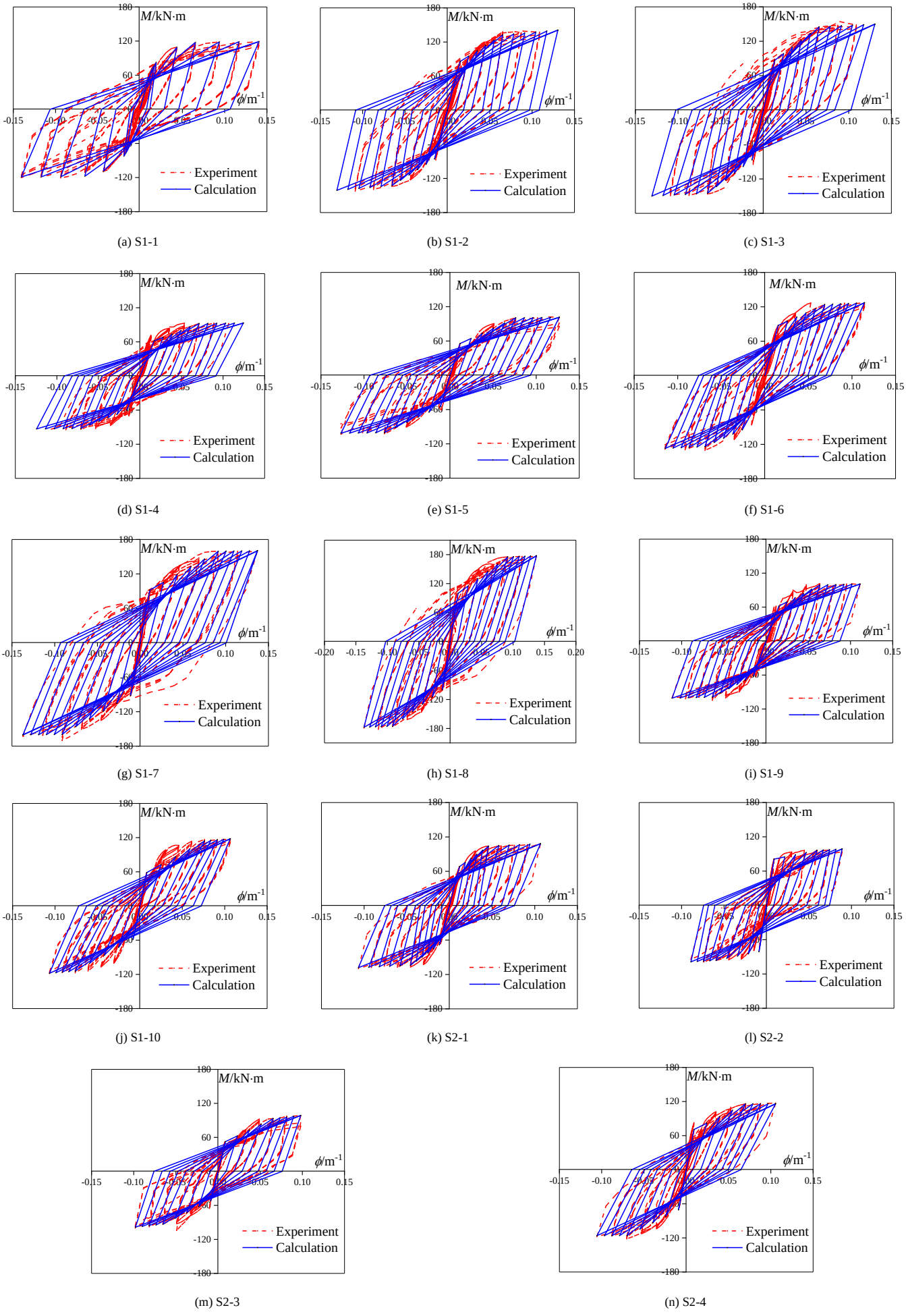

(a) S1-1 (b) S1-2 (c) S1-3

(d) S1-4 (e) S1-5 (f) S1-6

(g) S1-7 (h) S1-8 (i) S1-9

(j) S1-10 (k) S2-1 (l) S2-2

(m) S2-3 (n) S2-4

Fig. 12 Comparisons between the experimental $M-\phi$ hysteresis curves and theoretical $M-\phi$ hysteresis curves

5. Conclusions

In this paper, ten self-stressing SSACFST columns and four ordinary SSACFST columns (reference columns) under low cyclic loading are tested. The effects of axial compression ratio, diameter-thickness ratio, shear-span ratio and expansion rate of SSAC on seismic performances are analyzed.

(1) Under the cyclic loading, the failure mode of self-stressing SSACFST columns with high shear-span ratio exhibits bending failure, while that of the columns with low shear span ratio is bending-shear failure. The other three experimental parameters have insignificant influence on final failure mode.

(2) All specimens initially show elastic response, moment and curvature increase linearly. The $M-\phi$ hysteretic curves gradually deviate from the linearity, the hysteretic curves exhibit remarkable fusiform shape and show satisfactory energy dissipation capacity. The $M-\phi$ hysteretic curves present slight pinch phenomenon at the late loading stage.

(3) With the enhancement of axial compression ratio or expansion rate of SSAC, the peak moment of specimens increases. The increase of shear-span ratio or diameter-thickness ratio decreases the peak moment. The peak curvature of specimens decreases as axial compression ratio increases, while it increases as shear-span ratio increases. The impacts of diameter-thickness ratio and expansion rate of SSAC on the peak curvature are marginal.

(4) A simplified model for predicting the $M-\phi$ skeleton curves of self-stressing SSACFST columns is suggested based on tri-linear skeleton model of CFST members. The hysteretic rules of the specimens are also proposed by analyzing the features of the hysteretic curves. A model for evaluating the moment-curvature behavior of self-stressing SSACFST columns under low cyclic loading is established and validated the experimental results with good agreement.

Acknowledgements

This study was sponsored by the National Natural Science Foundation of China (No.52078001), Outstanding Youth Fund of Anhui Province (No. 2008085J29), Key Research and Development Project of Anhui Province (No. 2022i01020005), Major Science and Technology Project of Anhui Province (No. 202203a07020005), Key Laboratory of Metallurgical Emission Reduction & Resources Recycling (Anhui University of Technology), Ministry of Education (No. JKF22-08).

References

[1] Guo, J. L., Bao, Y. P. and Wang, M., "Steel slag in China: Treatment, recycling, and management", Waste Manage, 2018, Vol. 78, No. 8, pp. 318-330.
[2] Guo, Y., Xie, J., and Zhao, J., "Utilization of unprocessed steel slag as fine aggregate in normal- and high-strength concrete", Constr Build Mater, 2019, Vol. 204, No. 20, pp. 41-49.
[3] Palankar, N., Ravi Shankar, A.U., and Mithun, B.M., "Durability studies on eco-friendly concrete mixes incorporating steel slag as coarse aggregates", Clean Prod, 2016, Vol. 129, No. 15, pp. 437-448.
[4] Saxena, S., Tembhurkar, A.R., "Impact of use of steel slag as coarse aggregate and wastewater on fresh and hardened properties of concrete", Constr Build Mater, 2018, Vol. 165, pp. 126-137.
[5] Lai, M. H., Zou, J., Yao, B., Ho, J.C.M., Zhuang, X., and Wang, Q., "Improving mechanical behavior and microstructure of concrete by using BOF steel slag aggregate", Constr Build Mater, 2021. Vol. 277, 122269.
[6] Netinger, I., Bjegović, D. and Vrhovac, G., "Utilization of steel slag as an aggregate in concrete", Fatigue Fract Eng M, 2011, Vol. 44, No. 9, pp. 1565-1575.
[7] Anastasiou, E., Filikas, K.G. and Stefanidou, M., "Utilization of fine recycled aggregates in concrete with fly ash and steel slag", Constr Build Mater, Vol. 50, No. 1, pp. 154-161.
[8] Gencel, O., Karadag, O., and Oren, O. H., "Steel slag and its applications in cement and concrete technology: A review", Constr Build Mater, 2021, Vol. 283, 122783.
[9] Qasrawi, H., Shalabi, F. and Asi, I., "Use of low CaO unprocessed steel slag in concrete as fine aggregate", Constr Build Mater, 2009, Vol. 23, No. 2, pp. 1118-1125.
[10] Maslehuddin, M., Sharif, A.M., Shameem, M., Ibrahim, M. and Barry, M. S., "Comparison of properties of steel slag and crushed limestone aggregate concretes", Constr Build Mater, 2003, Vol. 17, No. 2, pp. 105-112.
[11] Wang, Q., Yan, P., "Hydration properties of basic oxygen furnace steel slag", Constr. Build. Mater, 2010, Vol. 24, No. 7, pp. 1134-1140.
[12] Wang, X., Ni, W., Li, J.J. and Zhang, S. Q., Michael, H. and Rodrigo. P., "Carbonation of steel slag and gypsum for building materials and associated reaction mechanisms", Cement Concrete Res, 2019, Vol. 125, No. 11, 105893.
[13] Huo, B. B., Li, B. L., Huang, S. Y., Chen, C., Zhang, Y. M. and Banthia, N., "Hydration and soundness properties of phosphoric acid modified steel slag powder", Constr Build Mater, 2020, Vol. 254, No. 11, 119319.
[14] Wang, Q. Wang,, D.Q. and Zhuang, S.Y., "The soundness of steel slag with different free CaO and MgO contents", Constr Build Mater, 2017, Vol. 151, pp. 138-146.
[15] Ukanwa, K.U., Clifton, C.G., Lim, J. B. P., Hicks, S. and Sharma, U. K., "Numerical analysis of plain and steel fiber reinforced concrete filled steel tubular slender column", Adv Steel Constr, 2018, Vol. 14, No. 2, pp. 308-323.
[16] Wang, Q. L., Qu S. E., Shao, Y. B. and Feng, L. M., "Static behavior of axially compressed circular concrete filled cfrp-steel tubular (c-cf-cfrp-st) columns with moderate slenderness ratio", Adv Steel Constr, 2016, Vol. 12, No. 3, pp. 263-295.
[17] Ji, B., Fu, Z., Qu, T. and Wang, M., "Stability behavior of lightweight aggregate concrete filled steel tubular columns under axial compression". Adv Steel Constr, 2013, Vol. 9, No. 1, pp. 1-13.
[18] Xu, L.H., Zhou, P. H., Huang, L., Ye, J. Q. and Yu, M., "Performance of the high-strength self-stressing and self-compacting concrete-filled steel tube columns subjected to the uniaxial compression", Int J Civ Eng, 2018, Vol. 16, No. 9, pp. 1069-1083.
[19] Zhou, S. X., Ma, Y. and Sun, D. S., "The influence of bearing capacity of self-stressed cfst members for different strength grades and self-stressed magnitudes of concrete", Appl. Mech. Mater, 2012, No. 5, pp. 1546-1551.
[20] Li, N., Lu, Y. Y., Li, S. and Gao, D. Y., "Axial compressive behaviour of steel fibre reinforced self-stressing and self-compacting concrete-filled steel tube columns", Eng Struct, 2020, Vol. 222, No. 11, 111108.
[21] Chang, X., Huang, C. K. and Chen, Y. J., "Mechanical performance of eccentrically loaded pre-stressing concrete filled circular steel tube columns by means of expansive cement", Eng Struct, 2009, Vol. 31, No. 11, pp. 2588-2597.
[22] Yu, F., Yao, C., Hu, Y., Fang, Y., Niu, K., and Xiang, G. S., "Axial compressive behavior of self-stressing steel slag aggregate concrete filled steel tubular columns with bond-slip damage", Adv Steel Constr, 2020, Vol. 16, No.1, pp. 13–19.
[23] Shen, Q. H., Gao, H. B., Wang, J. F., and Wang, C. G., "Experimental study on performance of steel slag concrete filled elliptical steel tubular stub columns under axial load", J. Build Struct, 2021, Vol. 42, No.2, pp. 197-203 (in Chinese).
[24] Yu, F., Fang, Y., Zhang, Y. and Xu. L., "Mechanical behavior of self-stressing steel slag aggregate concrete filled steel tubular stub columns", Struct. Concr, 2020, Vol. 4, No. 20. pp. 1597-1611.
[25] Fang, Y., Yu, F., Zhang, Y. Xu, L. and Wang, X. L., "Mechanical behavior and bearing capacity calculation of self-stressing steel slag aggregate reinforced concrete filled circular steel tube columns", Acta Materiae compositae sinica, 2020, Vol. 37, No. 5, pp. 1211-1220 (in Chinese).
[26] Yu, F., Cao, Y., and Fang, Y.,"Mechanical behavior of self-stressing steel slag aggregate concrete filled steel tubular short columns with different loading modes", Struct, 2020, Vol. 26, pp. 947-957.
[27] Feng, P., Li, Z. Y., Zhang, S. B., and Yang, J. Q.,"Steel slag aggregate concrete filled-in FRP tubes: Volume expansion effect and axial compressive behaviour", Constr Build Mater, 2022, Vol. 318, 125961.
[28] GB/T50082-2009, Standard for test methods of long-term performance and durability of ordinary concrete, National Standards of People's Republic of China, Beijing, China, 2009.
[29] GB/T228.1-2010, Metallic materials-Tensile testing-Part 1: Method of test at room temperature, National Standards of People's Republic of China, Beijing, China, 2010.
[30] GB/T 50081-2019, Standard for test method of mechanical properties on ordinary the concrete strength of the concrete, National Standards of People's Republic of China, Beijing, China, 2019.
[31] Han, L.H., Concrete Filled Steel Tube Structure-Theory and Practice, Science Press, Bejing, China, 2016.
[32] Yao, C., Experimental study and theoretical analysis on seismic behavior of self-stressing steel slag aggregate concrete filled steel tubular columns, Master Thesis, Anhui University of Technology, 2020.
[33] Euro code 4, Design of Composite Steel and Concrete Structures, European Committee for Standardization, European, 2004.
[34] Zhong, S. T.,"Theoretical study on limit state of concrete filled steel tubular members under axial compression", Journal of Harbin Institute of Architectural Engineering, 1981, Vol. 1, No. 31, pp. 1-9 (in Chinese).